Counterion Condensation and Conformational Transitions of Polyelectrolytes Characterized by EPR Spectroscopy

Dariush Hinderberger, Gunnar Jeschke,* and Hans Wolfgang Spiess

Max-Planck-Institut für Polymerforschung, Postfach 3148, 55021 Mainz, Germany

Received July 15, 2002; Revised Manuscript Received October 15, 2002

ABSTRACT: Counterion condensation of multivalent, charged spin probes to highly charged cationic and anionic polyelectrolytes is characterized by CW and FT EPR spectroscopy. Line broadening and deviation from Lorentzian line shape in the EPR spectra of the spin probes are observed upon addition of the polyelectrolyte. These effects are due to dynamic electrostatic attachment of the counterions with exchange between the condensed and free states on a subnanosecond time scale. The spectral changes can be separated into a contribution due to slowdown of rotational dynamics and a contribution due to enhanced spin exchange. A drastic increase of the spin-exchange contribution is observed upon increasing the concentration of two anionic spin probes in aqueous solutions of the cationic polyelectrolyte poly(diallyldimethylammonium chloride), PDADMAC. This can be traced back to a counterion-induced chain collapse which is, however, not observed in mixtures of water with organic solvents of either higher (*N*-methylpropionamide) or lower (ethanol) permittivity. Simple polyelectrolyte theory, which considers solvents only as a dielectric continuum, cannot explain these findings. Screening of hydrophobic interactions between repeat units of the chain by the organic solvents is suggested as an explanation.

1. Introduction

Flexible polyelectrolytes—polymers with a large number of charged groups—have been known to adopt complex conformations in solution.[1,2] In solvents of "good" quality (temperature $T >$ Θ-temperature) polyelectrolytes exhibit extended conformations, at the Θ-temperature they can be described by a Gaussian chain, and in "poor" solvents ($T <$ Θ-temperature) they form compact, globular structures. In poor solvents but before the final collapse into a globule, the system of polyelectrolyte/solvent and counterions has been predicted to take on a conformation consisting of beads of monomers that are connected by strings of monomers.[4,5] Such intermediate *pearl necklace* structures are assumed to be stable due to a subtle balance between attractive hydrophobic interactions among the monomers and repulsive Coulomb forces of the charges, mediated through counterions. The effect of counterion condensation (electrostatic "condensation" of counterions to charges on the polyelectrolyte backbone) is seen as the key factor for understanding these complex structural changes.[1−6]

Besides the fundamental interest in this problem, polyelectrolyte−counterion interactions also play an important role in design and development of high-tech materials, such as polymer gels, and in many processes in molecular biology.[7] A prominent example is DNA transcription, for which the presence of divalent metal cations is of vital importance.[8]

In the dilute to semidilute regimes, which are the most simple regimes from a theoretical viewpoint, the well-established scattering techniques (light, X-ray, and neutron scattering) are not sufficient for a quantitative characterization of the investigated systems, mainly due to lack of sensitivity. Furthermore, these techniques may be influenced by small amounts of impurities (e.g., dust particles), which makes their use for such concentration regimes rather delicate. Electron paramagnetic resonance (EPR) methods,[9] being local, highly sensitive, and highly selective, may therefore be a valuable addition to the method arsenal. In particular, ionic spin probes can provide detailed information on structure and dynamics of polymer systems containing charges.[10−13]

In this work we introduce the use of spin probes with two or three charges, such as triarylmethyl trianion radicals, nitroxide dianion radicals, and divalent transition-metal ions, to investigate electrostatic interactions and changes in the conformations of the polyions. The local environment of spin probes is characterized by CW- and FT-EPR at X-band (∼9.7 GHz) and W-band (∼94 GHz) in fluid solution. The paper is organized as follows. First, we present evidence that spectral changes of ionic spin probes upon addition of polyelectrolytes are due to dynamic electrostatic attachment. Second, we describe the observed phenomena for the nitroxide dianion probe in water and two solvent mixtures with higher and lower dielectric constant and for variation of the ionic strength and for the trianion and transition metal ion probe in water. Third, we present possible scenarios for the dynamic attachment and distribution of counterions based on exclusively electrostatic effects and on conformational changes coupled with the electrostatic effects and discuss our results in the context of these scenarios.

2. Materials and Methods

As spin probes (Scheme 1) we used Fremy's salt dianion (potassium nitrosodisulfonate), FS, with a purity of 97% (ICN Biomedicals), triarylmethyl trianion, TAM (sodium salt, gift from Nycomed Innovations AB, Sweden), and $MnCl_2$ with a purity of 98% (Fluka).

As a cationic polyelectrolyte we chose poly(diallyldimethylammonium chloride), PDADMAC, with an M_W of 240 000 (Polysciences, Inc.), and as an anionic polyelectrolyte poly(sodium 4-styrenesulfonate), PSS, with average M_W of 1 000 000 (Aldrich Chem. Co.). All chemicals were used as received.

The solvent systems were deionized Milli-Q water (permittivity: $\epsilon_r = 80$ at 293 K), 50 vol % ethanol (Riedel-de Haën)/50 vol % water (density $\rho = 0.895$, approximate $\epsilon_r = 50$ at 293 K), and 70 vol % *N*-methylpropionamide (Aldrich Chem. Co.)/30 vol % water (NMPA/H_2O, $\rho = 0.951$, approximate $\epsilon_r = 140$ at 293 K). Unless noted otherwise, small amounts of KOH were added to adjust the solution to pH ∼8. The spin probe concentration was usually fixed at 0.5 mM, and polyelectrolyte

10.1021/ma021105k CCC: $22.00
Published on Web 11/21/2002

Scheme 1. Molecular Structures of Charged Spin Probes and Polyelectrolytes Used in This Study[a]

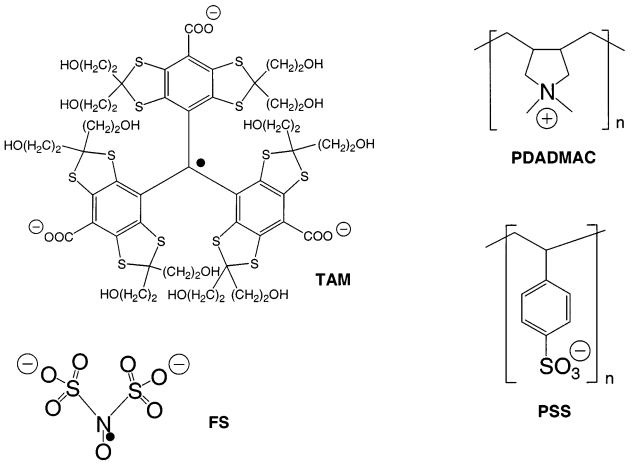

[a] TAM = triarylmethylradical trianion; FS = Fremy's salt dianion; PDADMAC = poly(diallyldimethylammonium chloride); PSS = poly(sodium 4-styrenesulfonate).

concentration was varied from 3 mM (in monomeric units) to at least 140 mM. Data are presented as a function of the ratio R of spin probes to polymer repeat units, so that no assumption on the actual number of repeat units per chain, and thus on M_n, had to be made.

EPR spectra at X-band (~9.7 GHz) were measured on a Bruker ELEXSYS 580 spectrometer using an AquaX inlet and a rectangular cavity (4103TM, Q values typically ~3000). FT EPR spectra at X-band were detected on the same spectrometer with the same probehead but with a sample volume of 20 to 40 μL in quartz tubes of 4 mm outer diameter (Wilmad Corp.).

EPR spectra at high-field/high-frequency (W-band, ~94 GHz) were recorded on a Bruker ELEXSYS 680 spectrometer with a Bruker TeraFlex probehead. Sample volumes of 1−3 μL were filled in homemade rounded-bottom Suprasil capillaries (inner diameter 0.7 mm, outer diameter 0.87 mm, Wilmad Corp.), which were then sealed with fast-drying glue.

EPR spectra were fitted either by the fitting program described by Robinson et al.[14] (extraction of average hyperfine couplings $\bar{a}$) or by a home-written program, which takes into account that line widths may be broadly distributed.

In analogy to studies of relaxation times in disordered systems, our program assumes that relaxation can be described by a stretched exponential.[15] The time-domain signal for a single line with resonance offset ω_i, characteristic transverse relaxation time T_2, and stretch factor x is then given by

$$V_i(t) = \exp\left(-\frac{t}{T_2}\right)^x \exp(i\omega_i t) \qquad (1)$$

The time-domain signals of the three lines of the nitroxide spectrum are added, the sum signal is Fourier transformed, and the CW spectrum is obtained by pseudomodulation[16] with the same modulation amplitude as used in the experiments. This approach provides a quantification of the non-Lorentzian lines with a minimum number of fit parameters and without making any assumptions on the physical process leading to relaxation.

Lorentzian line widths are calculated by $\Delta B = [0.412\ (G/\mathrm{MHz}) \times T_2^{-1}]$.[17] Rotational correlation times were approximated by using an approach by Goldman et al.[18] with the line width parameter $B = (\Delta B(m_I{=}-1) - \Delta B(m_I{=}1))/2$, where $m_I = -1$ corresponds to the high-field line and $m_I = 1$ to the low-field line.

3. Results

3.1. Electrostatic Attachment of Spin Probes. According to the basic theory of polyelectrolyte−counterion interaction introduced by Manning,[3] attachment of multivalent counterions to the polyelectrolyte backbone should be preferred to attachment of monovalent counterions for reasons of maximizing the entropy of the complete system. Therefore, we use di- or trivalent counterions as spin probes. The somewhat misleading term *electrostatic condensation* is established for this kind of attachment, but we point out that a given counterion is not permanently attached to a specific backbone charge in fluid solution. The *dynamic* attachment of a charged spin probe should influence its EPR spectrum, as parameters such as line widths, line shapes, and hyperfine couplings are known to be very sensitive toward even small changes in the molecules' surroundings.[19−21]

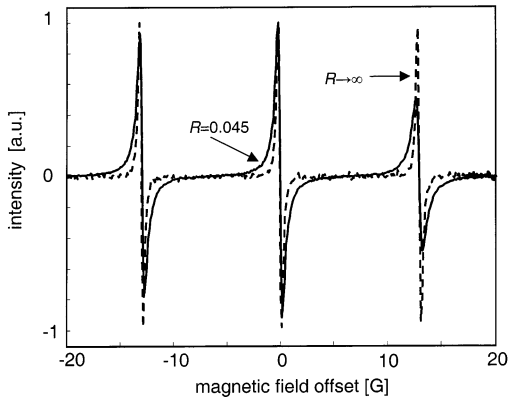

Figure 1. X-band (9.77 GHz) EPR spectra of FS in aqueous solution at two different spin probe/PDADMAC ratios R.

Indeed we find that addition of oppositely charged polyelectrolyte to solutions of multivalent spin probes in pure solvent causes a marked increase in the peak-to-peak line widths. Typical data for the probe FS in water/PDADMAC are shown in Figure 1. To exclude effects other than electrostatic ones as the reason for this, we measured reference samples of the *neutral* spin probe 4-oxo-2,2,6,6-tetramethylpiperidine-1-oxyl with cationic and anionic polyelectrolyte, the cationic spin probe 4-trimethylammonium-2,2,6,6-tetramethylpiperidine-1-oxyl with the cationic polyelectrolyte PDADMAC, and FS with the anionic polyelectrolyte PSS for such concentration ratios where maximum line broadening was observable for the systems under investigation. No line broadening could be detected in any of the reference systems (spectra not shown). Hence, the change in viscosity on adding the polyelectrolyte cannot be held responsible for the observed drastic spectral changes. In fact, no impact of viscosity was found even for those samples containing the highest amounts of polyelectrolyte (spectra not shown). This is conclusive evidence that dynamic electrostatic attachment is the main cause of the observed spectral changes.

3.2. Fremy's Salt + PDADMAC. We systematically varied the spin probe/polyelectrolyte ratio R from 0.003 to 0.135 in three different solvent systems (H_2O: ϵ_r = 80; NMPA/H_2O: ϵ_r = 140; ethanol/H_2O: ϵ_r = 50). In Figure 2a−c the general trends of the line widths in the three solvents are displayed. Line broadening is most pronounced for the pure aqueous solution spectra but is also significant for the solvent mixtures. This broadening can be traced back partially to a change in the rotational correlation times (Figure 2d). The behavior for the solutions in pure water is qualitatively different from the behavior for solvent mixtures. Furthermore,

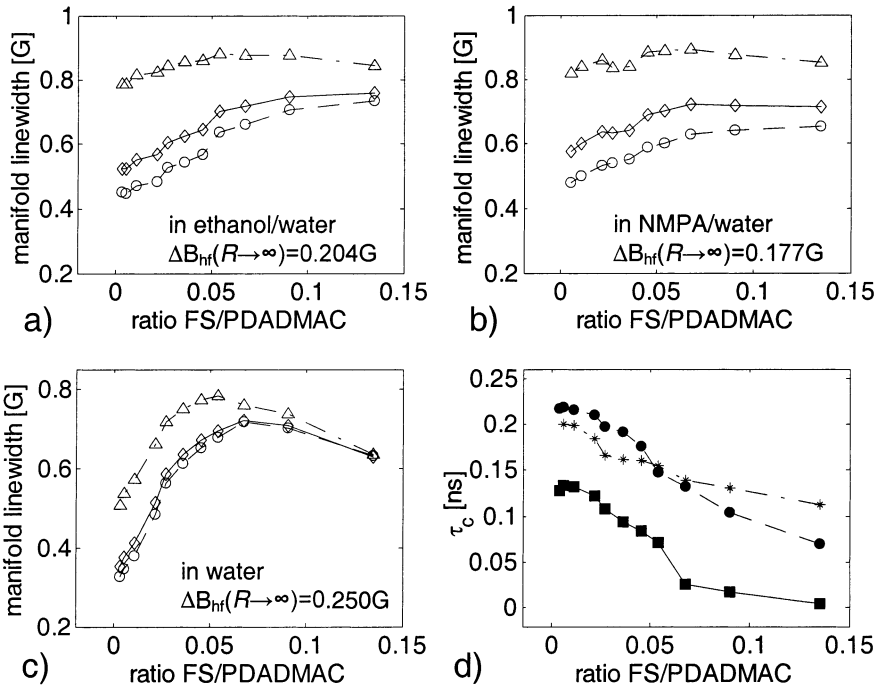

Figure 2. Line widths and rotational correlation times (EPR frequency: 9.77 GHz) for spin probe FS as a function of FS/PDADMAC ratio R in three different solvents. Parameter uncertainties are within marker size, and lines are meant as a guide to the eye. (a) In 50% ethanol/50% water. (b) In 70% NMPA/30% water. (c) In 100% water. ΔB_{hf}: high-field line width for $R \rightarrow \infty$; diamonds/solid lines: low-field manifolds; circles/dashed lines: center-field manifolds; triangle/dash−dot lines: high-field manifolds. (d) Rotational correlation times calculated from line width differences in all three solvents. Filled squares/solid line: in water ($\tau_c(R\rightarrow\infty) = 0.004$ ns); filled circles/dashed line: in ethanol/water ($\tau_c(R\rightarrow\infty) = 0.005$ ns); asterisk/dash−dot line: in NMPA/water ($\tau_c(R\rightarrow\infty) = 0.009$ ns).

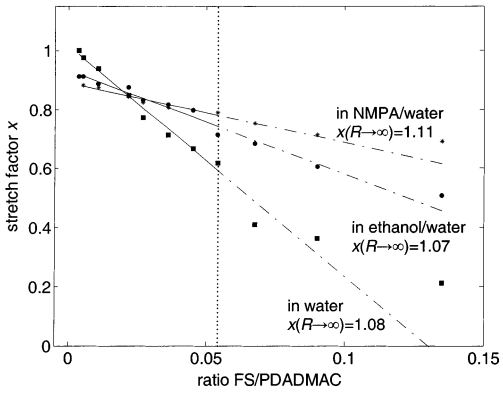

Figure 3. Characterization of the relaxation line distribution in FS X-band (9.77 GHz) EPR spectra by stretch factors x as a function of FS/PDADMAC ratio R in three solvents (see eq 1). Straight lines are linear fits including data points up to $R = 0.06$ (marked by vertical dotted line; extrapolation of the fit: dash−dot lines). Strong deviation from linearity can only be observed in water. Linear fits: in water: $x = 1.015-7.790R$; in ethanol/water: $x = 0.933-3.533R$; in NMPA/water: $x = 0.889-2.019R$.

for the ethanol/water and NMPA/water mixtures not only the trends coincide but also the absolute values are similar. The same applies to the stretch factors gained from simulations according to eq 1, which are presented in Figure 3 for all three solvent systems. These stretch factors are a measure of the width of distribution of the line widths.

We also investigated changes in the isotropic hyperfine coupling constant $\bar{a}$ for solutions of FS and PDADMAC in the three different solvents (not shown). All three systems show a rather pronounced drop in $\bar{a}$ of ca. 0.05 G even when only a small amount of polyelectrolyte is added to the solution. However, no further significant changes are observed when the PDADMAC concentration is increased. As the isotropic hyperfine constants for FS depend more strongly on temperature than for other nitroxide spin probes, the measured small variations might be influenced significantly by inevitable temperature fluctuations. For this reason we refrain from discussing this parameter in detail for the three PDADMAC concentration series.

W-band (94 GHz) EPR spectra of FS/PDADMAC solutions with different R values were also recorded. Because of larger anisotropy of the electron−Zeeman interaction, in this frequency regime the slowing of rotational motion upon dynamic electrostatic attachment of FS probes dominates the spectra. This results in smaller effects of the more interesting exchange interaction on the line widths of the W-band EPR spectra.

FS + PDADMAC in H_2O. The trends for line widths and rotational correlation times (Figure 2c) can be described in terms of three different regimes. Upon increase of R from 0.0036 to 0.04 line widths increase strongly. A flat maximum region is attained at ratios between 0.04 and 0.06, and a further increase of R leads to a decrease of line widths with a more moderate slope. Rotational correlation times (Figure 2d) are almost invariant (0.13 ns) for $R < 0.03$ and then decrease linearly up to a ratio of 0.05. The correlation times for ratios 0.06 and higher also decrease linearly, but with a very moderate slope.

Stretch factors cover a broad range from around 1 (at no polyelectrolyte contents) to as low as 0.2 for $R = 0.135$. Two different trends can be distinguished: for $R < 0.06$ they follow a linear trend (added as least-squares fit in Figure 3) from which they then deviate by decreasing more slowly than before.

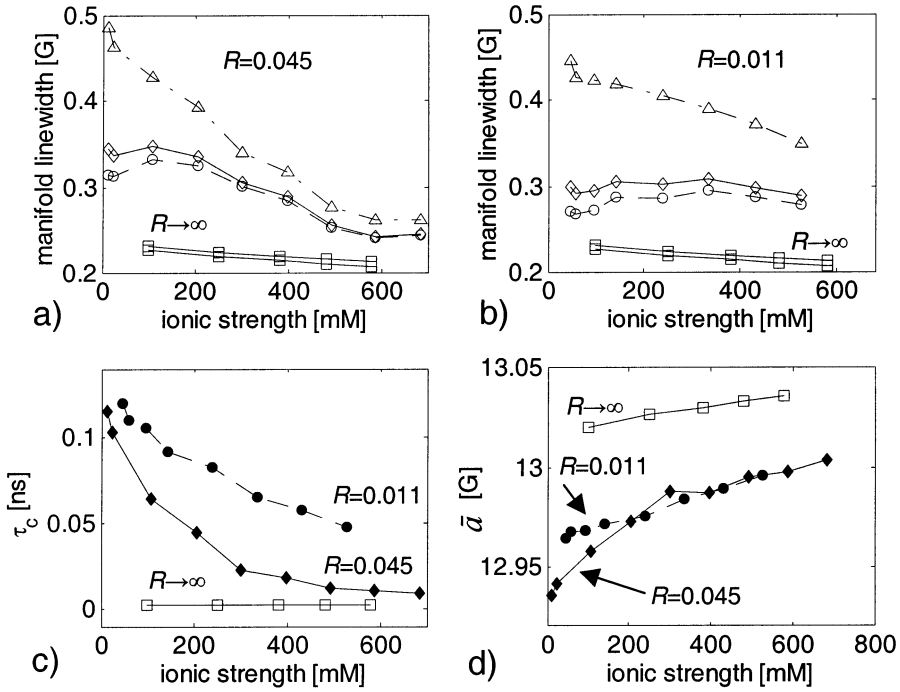

Figure 4. X-band (9.77 GHz) EPR data of two samples with different FS/PDADMAC ratio R in water as a function of ionic strength (addition of NaCl). (a) Line widths of the sample with $R = 0.045$. (b) Line widths of sample with $R = 0.011$; diamonds/solid lines: low-field manifolds; circles/dashed lines: center-field manifolds; triangles/dash−dot lines: high-field manifolds. (c) Rotational correlation times of respective samples. (d) Hyperfine coupling constants $\bar{a}$. All four figures also show the data for the reference sample without PDADMAC ($R \rightarrow \infty$) as open squares. Simulation uncertainties are within marker size, and lines are meant as a guide to the eye.

FS + PDADMAC in 50% H_2O/50% Ethanol. The line width increase with increasing R is also linear (Figure 2a), but not as steep as for purely aqueous samples. At $R \approx 0.06$, a plateau is reached, and no distinct maximum is observed. The absolute values of rotational correlation times are higher than for aqueous solution (Figure 2d) and decrease 3-fold from a value of 0.24 ns for low R to 0.07 ns at high R. Stretch factors x range from values slightly lower than 1 at no polyelectrolyte content to 0.5 for $R = 0.135$. A linear fit is in good agreement with the data throughout the whole polyelectrolyte concentration range (see Figure 3) and yields a slope that is less than half that of the respective fit for pure water samples.

FS + PDADMAC in 70 vol % NMPA/30% H_2O. Comparison of the respective plots of the line widths and rotational correlation times for water/ethanol and water/NMPA mixtures (Figure 2a,b,d) shows that not only the trends for the parameters are the same but that even the absolute numbers of line widths and τ_c are approximately the same. Line widths increase linearly with R and then reach a plateau for $R \approx 0.06$, whereas the τ_c decrease from 0.20 to 0.11 ns in the range $R = 0-0.14$.

FS + PDADMAC: Variation of Ionic Strength by Addition of NaCl. Two samples of FS and PDADMAC in water were selected for studying the effect of ionic strength on the EPR spectra and parameters: the sample with a ratio $R = 0.011$ (PDADMAC concentration $c = 46$ mM) and the one with a ratio $R = 0.045$ (PDADMAC concentration $c = 11$ mM).

The ratio 0.011 corresponds to the regime where in the absence of additional salt line widths increase linearly and the ratio of 0.045 to the regime where they attain their maxima (Figure 2c). Ionic strength was varied by adding NaCl to final concentrations from 0 to 600 mM. Figure 4a,b depicts the effect that increasing ionic strength has on the line widths, whereas Figure 4c shows the effect on τ_c.

For the sample with $R = 0.011$ (Figure 4c) rotational correlation times decrease linearly with increasing salt content, reaching slightly less than half the value of the salt-free solution at an ionic strength of 500 mM. Closer inspection shows that this decrease is manifested in a linear decrease of the high-field manifold line width, while the low-field and center-field manifold line widths remain roughly constant. Substantially different behavior is observed for the system with a ratio $R = 0.045$. Here, the addition of NaCl up to an ionic strength of 300 M leads to a faster, nonlinear decrease of τ_c, which changes into a slow decrease for even higher ionic strengths. Furthermore, the center-field and low-field manifold line widths reach maxima for ionic strength of approximately 120 mM and decrease slowly but significantly for higher ionic strengths. For the system with $R = 0.011$, the hyperfine couplings also increase in a linear manner (Figure 4d). The slope is similar to that of a reference sample not containing polyelectrolyte. For $R = 0.045$ again two different regimes are observed. Up to an ionic strength of 300 mM, $\bar{a}$ increases from a lower starting value with a steeper slope than for the reference sample, but for even larger ionic strengths the trend changes and the two curves virtually coincide.

3.3. TAM + PDADMAC in H_2O. For aqueous solutions of the TAM trianion ($c = 0.4$ mM) with variable concentrations of PDADMAC, spectra were recorded by FT EPR, as this method requires less sample volume than CW EPR with the AquaX inlet and provides perfectly phased spectra. Because of lack of excitation bandwidth, the same method could not be applied to the much broader spectra of the FS probe. Typical TAM spectra are presented in Figure 5a; the dependence of

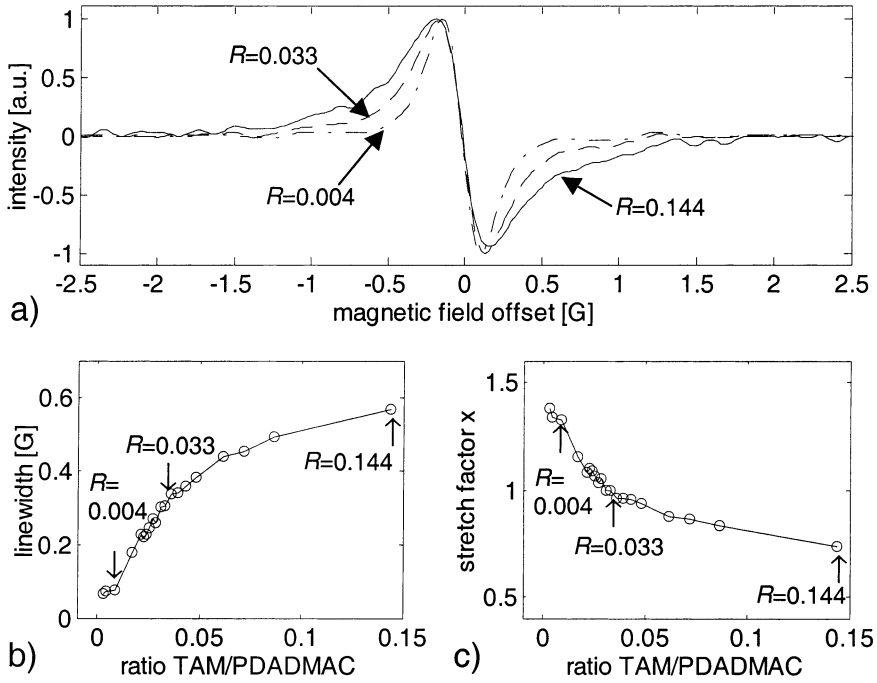

Figure 5. X-band (9.67 GHz) FT-EPR spectra and simulation parameters of TAM in aqueous solution as a function of TAM/PDADMAC ratio R: (a) X-band EPR spectra; (b) line widths from fitting of spectra to eq 1 ($\Delta B(R\rightarrow\infty) = 0.04$ G); (c) stretch factors from fitting of spectra to eq 1 ($x(R\rightarrow\infty) = 1.48$). Simulation uncertainties are within marker size, and lines are meant as a guide to the eye.

the line width ΔB and stretch factor x on the ratio R of TAM/PDADMAC is shown in Figure 5b,c.

A steep line width increase is observed when R is raised in the interval $0.01 \leq R \leq 0.04$. For $R > 0.04$ the line width increase levels off, and for $R < 0.01$ the line widths slowly approach the value observed without polyelectrolyte. Note that the stretch factor $x = 1.48$ for the probe in pure water deviates significantly from unity, which means that the line shape is not purely Lorentzian. Nevertheless, the *trend* of line shape stretch factors for TAM is similar to the trend for FS; namely, the value observed in pure solvent is again approached for *high* polyelectrolyte concentrations (low values of R).

W-band (94 GHz) CW EPR spectra of TAM/PDADMAC displayed even stronger effects on line width and line shape upon variation of R. However, extensive series of measurements of aqueous solutions are tedious to perform at W-band frequency, so that we solely focus on X-band EPR data in the present study.

3.4. $Mn(H_2O)_6^{2+}$ + PSS in H_2O. The FS and TAM probes are spectroscopically convenient and can provide extensive information on the polyelectrolyte/counterion interaction. However, they are poor mimics for the small spherical ions that are used in other experimental studies and that are assumed in most theoretical work. Thus, we also checked whether EPR spectra of the divalent transition metal ion Mn^{2+} are sensitive to the presence of an oppositely charged polyelectrolyte (PSS). High-field/high-frequency spectra (W-band, ~94 GHz) of aqueous solutions of $MnCl_2$ ($c = 2$ mM) for $R = 0.05$ and a pure $MnCl_2$ solution ($R \rightarrow \infty$) are presented in Figure 6a. The detailed plot (Figure 6b) shows clearly that addition of the polyelectrolyte induces not only an increase in peak-to-peak line width but also a change in the line shape similar to the one observed for FS and TAM probes.

Though more extensive quantitative results for this system have yet to be gathered, this indicates that the observations made with the FS and TAM probes may also be relevant for smaller spherical multivalent counterions.

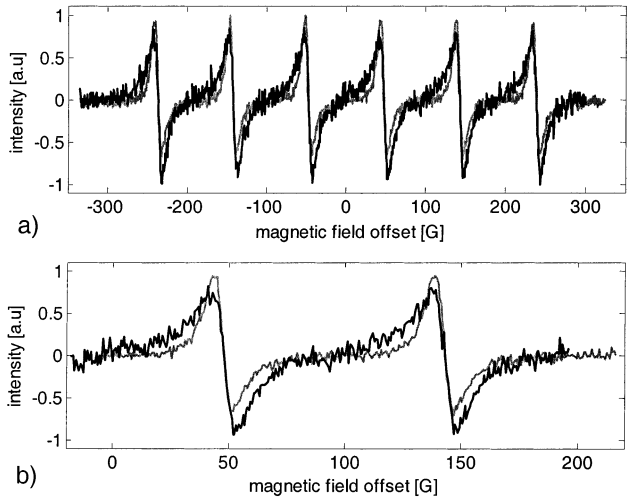

Figure 6. High-field/high-frequency (94 GHz) EPR spectra of Mn^{2+} of two different Mn/PSS ratios R in aqueous solution. Black line: $R = 0.05$; gray line: $R \rightarrow \infty$ (pure water). (a) Full spectra. (b) Detailed plot of lines 4 and 5 of the spectra.

4. Discussion

Fundamental Models. In the basic theory of polyelectrolyte/counterion interactions introduced by Manning the polymer is approximated as a linear extended chain, and the distribution of the pointlike counterions is considered as a function of their distance r from the chain.[1−3]

The central parameter ξ of this theory (Manning parameter) determines whether counterions are condensed to the polymer backbone or not:

$$\xi = l_B \frac{1}{b} = \frac{e^2}{4\pi\epsilon_0\epsilon_r k_B T}\frac{1}{b} \quad (2)$$

where l_B is the Bjerrum length, b is the average spacing of charged sites on the polymer, e is the electron charge, k_B is the Boltzmann constant, and T is the temperature. The product $\epsilon_0\epsilon_r$ is the absolute permittivity of the solvent, where ϵ_r is the dimensionless relative permittivity (dielectric constant).

If the Manning parameter is greater than the inverse of the counterion valence ($\xi \geq |Z_i|^{-1}$), condensation of part of the counterions to the chain is energetically favored. Such counterion condensation screens the repulsive electrostatic interactions between repeat units, so that a conformational change of the polymer from the extended to a collapsed conformation may occur. Counterion condensation can be controlled by additional electrostatic screening due to addition of low-molecular-weight salts. For the screened electrostatic potential one obtains[22]

$$\phi_1(r) = \frac{q_1 e^{-\kappa(r-a)}}{\epsilon_0\epsilon_r r(1+\kappa a)} \quad \text{for } r > a \quad (3)$$

where a is the radius of the ionic group. With increasing ionic strength I, which is proportional to the square root of κ, the screening of the interaction becomes more effective. Applying eq 2 to the PDADMAC and PSS systems is possible if a measure for the distance b of the charges on the polymer backbone is available. Force field (MMFF94) calculations for the optimization of geometry were performed for fully extended chains of 32 repeat units of PDADMAC and PSS. For PDADMAC this yields a value of $b = 8.5$ Å, and for PSS $b = 7.8$ Å. The Bjerrum length in water at 291 K is 7.2 Å, so that one obtains ξ(PDADMAC) = 0.85 and ξ(PSS) = 0.92. In water, the Manning parameter for fully extended chains of PDADMAC and PSS is thus above the critical value of condensation for the probe ions ($|Z_i|^{-1} = {}^1/_2$ and ${}^1/_3$, respectively), whereas it is close to, but below, the critical value for monovalent counterions. In practice, the chains may not be fully extended and effective ξ values may be larger.

Numerical calculations of the distribution equilibrium of bound and free monovalent counterions around a cylindrical macroion were carried out following a simple two-state model.[2] Again assuming fully extended chains such calculations suggest that for PDADMAC in the whole concentration range studied the fraction of bound monovalent counterions is between 15% and 20% and for PSS ca. 25%.

In section 3.1 it was concluded that the multivalent probe ions, which constitute only a small fraction of all counterions, are condensed to the polyelectrolyte molecules. This is also consistent with the argument that in a mixture of counterions the ξ parameter reaches the critical value for condensation earlier for multivalent than for monovalent counterions.[2] Hence, we expect that the multivalent probe ions expel parts of the bound monovalent counterions.

Counterion Condensation. Experimental rotational correlation times of the dianion probe FS in PDADMAC solutions show that the rotational mobility of the probes is significantly hindered upon addition of the polyelectrolyte, but not to such a degree that the attachment could be categorized as tight binding. This agrees with our expectation that effective condensation has to be viewed as a "dynamic" attachment−detachment equilibrium. Furthermore, it proves that the exchange between bound and free states is fast on our experimental EPR time scale (∼1 ns). At room temperature the spin probes have sufficient thermal energy to leave the area directly around the backbone, before they again approach the polyelectrolyte charges.

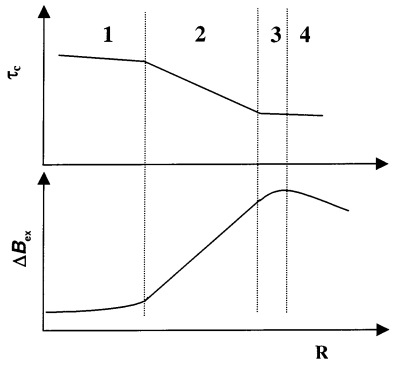

Figure 7. Sketch of the rotational correlation times (upper part) and spin-exchange contribution to the line width (lower part) dependence on R for case I. The line broadening induced by spin exchange is proportional to the local concentration. The four regimes marked 1−4 are explained in the text.

There are two physical effects contributing to the observed behavior of spectral parameters. First, rotational dynamics are changed, as the counterions are transiently immobilized on the polymer backbone, which leads to higher τ_c values. This effect can only be extracted from spectra of FS probes, as for the TAM trianion the anisotropy of g and hyperfine tensors is too small. Second, spin-exchange coupling, which stems from actual physical overlap of the electron bearing molecular orbitals during collisions of two probe molecules, is indicative of higher local concentrations of probe molecules in the vicinity of the polyelectrolyte backbone.[23] The peculiar line shape can be traced back to a heterogeneity of spin probe concentration on the time scale of the collisions. In the case of TAM, line width increase upon addition of polyelectrolyte is exclusively due to such spin-exchange interaction. Local concentrations in the vicinity of the chain are sensitive to conformational changes of that chain. The discussion of simultaneous changes in dynamics, local concentration, and heterogeneity of local concentration of the ionic spin probes should thus allow us to understand the differences in the data of the different systems presented above.

Case I: No Change of Polyelectrolyte Conformation with Increasing R. Assuming that condensed probe ions are homogeneously distributed along the polyelectrolyte chains, we obtain a simple semiquantitative model for the case of polyelectrolyte molecules that remain in an extended conformation throughout the whole range of probe/polyion ratios R. Figure 7 schematically depicts rotational correlation times and spin-exchange-induced line broadening for the expected four regimes. Note that in this scenario, as in our experiments, the probe concentration is fixed and increase of R is achieved by decrease of polyelectrolyte concentration.

At very low R the polymer concentration is so high that the *overlap regime* (regime 1 in Figure 7) for polymer chains is reached. Probes are dilute with respect to monomers and are exchanged between physically overlapping polyelectrolyte chains. The probe

molecules are confined to overlap regions, i.e., to domains of higher microviscosity. This leads to a strong slowdown of rotational dynamics. Local concentration of probe ions only weakly influences line widths in this regime, as the distribution of probes along the polymer chains is such that average distances between individual probe ions are very large, and thus spin-exchange broadening is less significant than broadening due to decreased mobility.

For higher values of R, polymer chains are dilute and probe ions are condensed to a single chain, and with increasing R, the local concentration of probe ions per macroion is raised linearly and spin-exchange broadening starts to dominate the line shapes. Line widths of spin probes thus enter a *linear increase regime* (regime 2 in Figure 7). In this regime, the rotational correlation time is expected to decrease slowly, as with increasing R the microviscosity of the domains of condensed probes is lowered.

At even larger R a *maximum regime* (regime 3 in Figure 7) is attained when the maximum value of probe molecules that can be attached to each single, extended chain is reached. This is the case once the product of the fraction of probe ions that is condensed (f_{cp}, assumed to be constant), and the ratio of multivalent probe ions to polyelectrolyte charges is close to unity: $f_{cp}R \approx 1$. At these values for R, rotational dynamics only decrease slowly.

Finally, further increase of R leads into a local concentration *decrease regime* (regime 4 in Figure 7), in which there are more probe ions than can be condensed to the polymer charges. Because of the dynamic character of the condensation process, probe ions reside in the detached state for increasingly longer periods of time with a further increase of R. Rotational dynamics now reach a plateau minimum value. For $R \rightarrow \infty$, all parameters (concentration, line widths, and rotational dynamics) are again congruent with those of pure probe molecules in the solvent.

Case II: Conformational Transition While Increasing R. The model of condensation of multivalent counterions and the plots of Figure 7 are modified if the condensation influences the conformational distribution of polyelectrolyte chains.

Assuming that in the *overlap regime* (regime 1) the small number of multivalent probe ions per chain is not sufficient to modify the extended chain conformations, the difference starts to come into play in the linear increase regime 2. In this scenario, condensed counterions increasingly alter those parts of the chain to which they are condensed. By screening the electrostatic repulsion of chain backbone charges, condensed probe ions induce collapses of certain domains, so that with increasing R there are higher contributions from collapsed domains of single chains to the overall distribution of conformations. Such a collapse transition was first proposed by Khokhlov[24] and later discussed by several authors.[25−29] Schiessel and Pincus pointed out that, depending on the microscopic properties of the chains and counterions, a first-order-type or second-order-type collapse transition may occur.[26]

Increasing R thus also leads to an *increase regime* like regime 2 in Figure 7, but with a much steeper increase of local concentration of probes as the chains are compacted. Probe counterions that interact with a globular domain of a macroion are confined to the smaller volume occupied by the collapsed chain and are thus more likely to collide with another probe counterion. This manifests itself in spin-exchange broadening of CW EPR spectra. Consequently, at a certain point the simple Manning theory for extended chains breaks down, and it becomes difficult to tell at which values for R the maximum corresponding to regime 3 in Figure 7 will be attained.

Despite this difficulty, it is reasonable to assume that for the (partly) collapsed chains binding of multivalent counterions is less favored than for fully extended chains. This assumption is based on two effects. First, if a chain is compacted, the loss of conformational entropy upon counterion binding is significantly higher. Second, in a collapsed domain of a polyelectrolyte chain there will be a close approach of multivalent probe ions at values for R, for which in the extended case average distances are much higher. Therefore, intermolecular interactions of like charged probe ions cannot be neglected any more. Thus, the maximum local concentration of multivalent counterions will be reached at lower ratios R. Ejection of a significant fraction of counterions from a collapsed polyelectrolyte chain is also suggested by the theoretical treatment of Kramarenko et al.[25] It is quite hard to predict rotational dynamics in this scenario because of the dynamic quality of the electrostatic attachment of counterions and also a change in the distribution of condensed and free probe ions as compared to the more simple scenario of Figure 7.

Interpretation of Data. *Effect of Different Solvents.* All data of FS and PDADMAC in ethanol/water as well as NMPA/water as solvents are fully consistent with case I of counterion condensation to chains in largely extended conformations described in the previous section. Line width plots (as a measure for exchange broadening and ultimately local concentration) in Figure 2a,b and respective rotational correlation times in Figure 2d indicate that for the range of R studied in this work FS/PDADMAC systems in those two solvents are in the *linear increase regime* of Figure 7. Note that the strongest contribution to the R-dependent rotational mobility, as it was suggested in the simple scenario of Figure 7 and also observed (Figure 2d), is an electrostatic effect. This has been verified by measuring reference samples of like-charged spin probes and polyelectrolytes, where no strong effects were observed (not shown). Furthermore, the dependence of stretch factors on R is strong evidence for this interpretation. With increasing R, stretch factors decrease linearly, starting from values that are close to those of the free probes in the solvents. This means that the width of the line width distribution (see eq 1) increases with increasing R, in accordance with the expectation that there are higher contributions to the overall spectral line width by detached probes on one hand and higher local concentrations on the other hand.

Remarkably, data of FS/PDADMAC in pure water fundamentally disagree with the expectations for case I. The line width increase with increasing R is much steeper than in the two other solvents, and there is a pronounced line width maximum. In case I (Figure 7), the line width maximum can only be expected at $R \geq |Z_i|^{-1}$ (as $f_{cp} \leq 1$) or higher, not at values as small as 0.06, as observed in water. In addition, stretch factors decrease strongly but linearly up to $R = 0.06$, where they depart from linearity and decrease more slowly. The data of FS/PDADMAC in water can, however, be explained consistently with a transition of PDADMAC

chains from extended to globular conformations. In other words, we observe a *counterion-mediated chain collapse*. This transition, which apparently has the character of a second-order transition, is completed at $R \approx 0.06$, when the "most densely packed" collapsed state is reached. In analogy to regime 4 in Figure 7, line widths decrease again with further increasing R values. The very broad distribution of line widths at these ratios (stretch factor as low as 0.2, see Figure 3) leads to the conclusion that with increasing R an increasing fraction of divalent probe ions resides in solution, where they experience collisions less frequently. In accordance with a scenario that includes a conformational transition of the polyelectrolyte, the mean line width therefore decreases after the collapse. This also indicates ejection of part of the counterions from the collapsed chain in agreement with predictions by Kramarenko et al.[25] and contradicting recent predictions by Solis and de la Cruz.[29] The estimate for τ_c may be not so reliable in this regime, as it is obtained by using the line width difference parameter B, which is ill-defined here due to the increasingly broad range of actual line widths that contribute. Therefore, we refrain from giving an interpretation of the deduced effective τ_c values for $R \geq 0.06$.

The fact that on one hand spectral parameters of FS probes for ethanol/water and NMPA/water as solvents behave very similarly, but on the other hand those parameters differ strongly from the pure water solvent values, is unexpected in the framework of basic polyelectrolyte theory. As outlined in the Introduction, ethanol/water ($\epsilon_r = 53$ at 293 K) is supposed to be a better solvent than water for the hydrocarbon backbone of the PDADMAC polyelectrolyte, whereas NMPA/water with its much higher permittivity ($\epsilon_r = 143$ at 293 K) is viewed as a poor solvent. So, in ethanol/water the PDADMAC chains should be less inclined to counterion-mediated collapse whereas in NMPA/water the collapsed state should be even more favorable than in water. Obviously, the basic theory, in which solvents are only considered as a dielectric continuum, fails to explain our observations. Apparently, the actual molecular structure of solvent molecules has to be taken into account. Despite the pronounced difference in permittivity, chemical structures of NMPA and ethanol molecules are similar. Both molecules consist of a polar part and a small nonpolar, alkyl part (propyl and ethyl groups, respectively). These alkyl groups may solvate hydrophobic groups of the polymer chains and may thus "screen" hydrophobic interactions. This screening of the hydrophobic monomer−monomer interaction diminishes a driving force for a counterion-mediated chain collapse. The polar groups of both solvents may at the same time interact with the quaternary ammonium groups, and the water molecules may be preferably located in the vicinity of the charges. Such preferential solvation was also suggested for phenol in ethanol/water mixtures on the basis of NMR data by Bagno et al.[30] Recently, a study of ethanol/water mixtures using neutron diffraction led to strong indications that such mixtures indeed show molecular segregation and ordering on a local level, which would also agree with our interpretation.[31] The main conclusion we draw is that permittivity (dielectric constant) of the solvent(s) is not the only significant and not even the most important characteristic of the solvent mixtures.

Effect of Addition of Low-Molecular-Weight Salt. The data for the FS/PDADMAC sample in water presented in Figure 4a−d clearly support the interpretation that at $R = 0.045$ (maximum region in Figure 2c) the chain adopts a different local structure than at $R = 0.011$ (linear increase region in Figure 2c). Only after the addition of 300 mM NaCl (ionic strength 320 mM) trends for the measured parameters of the 0.045 ratio sample resemble those of the 0.011 ratio sample. From the marked decrease of line widths and rotational correlation times as well as the increase of $\bar{a}$, we may conclude that at very high ionic strengths (500 mM and higher) the electrostatic interactions are screened to such an extent that electrostatic attachment of divalent spin probes is effectively suppressed. The strongly different, nonlinear dependence of the parameters on the ionic strength for the $R = 0.045$ system indicates that in this system the probes are in an environment significantly different from that for the $R = 0.011$ system, at least for $I < 300$ mM. This is clear evidence that the conformational ensembles at low I are different and that the difference is due to electrostatic effects. Our earlier conclusion that the counterions are bound to a collapsed polyelectrolyte chain at $R \approx 0.05$ is thus further supported. Moreover, this allows us to estimate that the PDADMAC conformational transition induced by FS counterions in water takes place in the range $0.01 < R < 0.04$.

TAM + PDADMAC in Water. The data shown in Figure 5a−c demonstrate that increasing R has a strong effect on TAM/PDADMAC spectra. Comparing TAM and FS, one has to bear in mind that TAM is a fairly rigid tristar-shaped trianion with an approximate distance of 1.1 nm between the charges.[32] This large distance between the charges may allow TAM to induce physical, *dynamical cross-links* between relatively remote repeat units of the same PDADMAC chain at higher R values (lower PDADMAC concentrations) and possibly between ionic groups of two distinct chains at low R (higher PDADMAC concentration). Such dynamical cross-links of condensed counterions should lead to different globular conformations than for FS. Hence, differences in the dependence of spectral parameters on R with respect to FS are not surprising.

Indeed, with increasing R we observe for TAM pronounced line width increases and approach to a line width maximum as well as a decrease in stretch factors and asymptotic approach to a stretch factor minimum. These findings also point toward higher contributions of probe-ion-induced collapsed conformations. The line width maximum of the "most densely packed" conformation is not reached at $R = 0.15$.

Pointlike Counterions: Mn^{2+} and PSS in H_2O. The line broadening in the $Mn(H_2O)_6^{2+}$ high-field/high-frequency EPR spectra upon addition of PSS points to a similar electrostatic attachment as observed for the anionic spin probes. At conventional frequency (X-band, 9.4 GHz) the spectrum of Mn^{2+} in pure water features very broad lines ($\Delta B_{pp} \approx 25$ G) due to relaxation induced by the zero-field splitting. Any further broadening induced by the polyelectrolyte is hard to detect (not shown). At W-band frequencies (94 GHz) the lines in the Mn^{2+} spectrum are much narrower ($\Delta B_{pp} \approx 9$ G), and effects can be seen clearly (Figure 6a,b).

We tentatively assign the observed broadening upon addition of PSS to deformation of the octahedral coordination of the Mn^{2+} ion with water molecules due to dynamic electrostatic attachment. This dynamic deformation of the coordination polyhedron modulates the

zero-field splitting, which is averaged in perfect octahedral symmetry except for a small contribution due to the hexadecapolar moment of the charge distribution. The modulation of the zero-field splitting in turn shortens the transverse relaxation time and thus broadens the line in an analogous manner as described by Strandberg and Westlund for Gd^{3+}.[33] Contributions to line widths by spin-exchange interaction are negligible for such broad lines. However, the detailed plot in Figure 6b illustrates that with PSS there is also a line shape change with broadening, especially at the wings of the lines. This again is an indication of a distribution of line widths and hence of relaxation times.

5. Conclusions

In this investigation we demonstrated for the first time that EPR on charged spin probes can provide information on counterion condensation to polyelectrolytes in fluid solution. We found that electrostatic attachment of counterions is dynamic with the exchange between the condensed and free states proceeding on a subnanosecond time scale.

We characterized the local environment of multivalent counterions that are electrostatically attached to polyelectrolytes by separating two physical effects that dominate the EPR spectra: rotational probe dynamics and exchange coupling, with the latter interaction being a measure of local probe concentration. The variation of these broadening contributions with the ratio of probe counterion to polyelectrolyte concentration suggests that counterion-mediated chain collapse takes place for PDADMAC in water. The critical ratio for this collapse could be estimated. For the first time it was shown experimentally that the structure of solvent molecules rather than only solvent permittivity influences polyelectrolyte conformation and conformational transitions. We attribute this to a significant screening of hydrophobic interactions between polyelectrolyte backbone monomers by solvent molecules with suitable groups. The basic assumption of most existing polyelectrolyte theory that considers solvents only as a dielectric continuum is in qualitative disagreement with our results. A more detailed characterization of the structure of polyelectrolyte/counterion aggregates should be possible by applying advanced pulse EPR methods at X-band and W-band frequencies to frozen glassy solutions of these systems. Such work as well as a more detailed and quantitative line shape analysis are now in progress. It is hoped that the newly available information on counterion dynamics and distribution will stimulate further theoretical research.

Acknowledgment. We thank Nycomed Innovations AB, Sweden, for generously supplying us with the TAM radical used in this study and C. Bauer for technical support. Financial support from the priority program "High-Field EPR in Biology, Chemistry and Physics" (SPP 1051) by the Deutsche Forschungsgemeinschaft (DFG) is gratefully acknowledged.

References and Notes

(1) Dautzenberg, H.; Jaeger, W.; Kötz, J.; Philip, B.; Seidel, C.; Stscherbina, D. *Polyelectrolytes*; Hanser-Verlag: München, 1994.
(2) Oosawa, F. *Polyelectrolytes*; Marcel Dekker: New York, 1971.
(3) Manning, G. S. *J. Chem. Phys.* **1969**, *51*, 924.
(4) Kantor, Y.; Kardar, M. *Phys. Rev. E* **1995**, *51*, 1299.
(5) Dobrynin, A. V.; Rubinstein, M.; Obukhov, S. P. *Macromolecules* **1996**, *29*, 2974.
(6) Micka, U.; Holm, C.; Kremer, K. *Langmuir* **1999**, *15*, 4033.
(7) Nishiyama, Y.; Satoh, M. *Polymer* **2001**, *42*, 3919. Kötz, J.; Kosmella, S.; Beitz, T. *Prog. Polym. Sci.* **2001**, *26*, 1199.
(8) Voet, D.; Voet, J. G. *Biochemistry*, 2nd ed.; J. Wiley & Sons: New York, 1995; Chapter 29, and references therein.
(9) Atherton, N. M. *Principles of Electron Spin Resonance*; Ellis Horwood Limited: New York, 1993.
(10) Xue, H. Q.; Bhowmik, P.; Schlick, S. *Macromolecules* **1993**, *26*, 3340.
(11) Tsagaropoulos, G.; Kim, J. S.; Eisenberg, A. *Macromolecules* **1996**, *29*, 2222.
(12) Schädler, V.; Franck, A.; Wiesner, U.; Spiess, H. W. *Macromolecules* **1997**, *30*, 3832.
(13) Cramer, S. E.; Jeschke, G.; Spiess, H. W. *Macromol. Chem. Phys.* **2002**, *203*, 182.
(14) Robinson, B. H.; Mailer, C.; Reese, A. W. *J. Magn. Reson.* **1999**, *138*, 199, 210.
(15) Scherer, G. W. *Relaxation in Glass and Composites*; Krieger: Malabar, FL, 1992; Chapter 4.
(16) Hyde, J. S.; Jesmanowicz, A.; Ratke, J. J.; Antholine, W. E. *J. Magn. Reson.* **1992**, *96*, 1.
(17) Schweiger, A.; Jeschke, G. *Principles of Pulse Electron Paramagnetic Resonance*; Oxford University Press: Oxford, 2001; p 97.
(18) Goldman, M. *J. Magn. Reson.* **2001**, *149*, 160.
(19) Ardenkjaer-Larsen, J. H.; Laursen, I.; Leunbach, I.; Ehnholm, G.; Wistrand, L. G.; Petersson, J. S.; Golman, K. *J. Magn. Reson.* **1998**, *133*, 1. Yong, L.; Harbridge, J.; Quine, R. W.; Rinard, G. A.; Eaton, S. S.; Eaton, G. R.; Mailer, C.; Barth, E.; Halpern, H. J. *J. Magn. Reson.* **2001**, *152*, 156.
(20) Käss, H.; MacMillan, F.; Ludwig, B.; Prisner, T. F. *J. Phys. Chem. B* **2000**, *104*, 5362.
(21) Bales, B. L.; Wajnberg, E.; Nascimento, O. R. *J. Magn. Reson. A* **1996**, *118*, 227.
(22) McQuarrie, D. A. *Statistical Mechanics*; HarperCollinsPubilshers: New York, 1976.
(23) Molin, Y. N.; Salikhov, K. M.; Zamaraev, K. I. *Spin Exchange: Principles and Applications in Chemistry and Biology*; Springer-Verlag: Berlin, 1980. Subczynski, W. K.; Hyde, J. S. *Biophys. J.* **1983**, *41*, 283.
(24) Khokhlov, A. R. *J. Phys. A* **1980**, *13*, 979.
(25) Kramarenko, E. Y.; Khokhlov, A. R.; Yoshikawa, K. *Macromolecules* **1997**, *30*, 3383.
(26) Schiessel, H.; Pincus, P. *Macromolecules* **1998**, *31*, 7935.
(27) Schiessel, H. *Macromolecules* **1999**, *32*, 5673.
(28) Shew, C. Y.; Yethiraj, A. *J. Chem. Phys.* **1999**, *110*, 676.
(29) Solis, F. J.; de la Cruz, M. O. *J. Chem. Phys.* **2000**, *112*, 2030.
(30) Bagno, A.; Campulla, M.; Pirana, M.; Scorrano, G.; Stiz, S. *Chem. Eur. J.* **1999**, *5*, 1291.
(31) Dixit, S.; Crain, J.; Poon, W. C. K.; Finney, J. L.; Soper, A. K. *Nature (London)* **2002**, *416*, 829.
(32) Value from DFT (ADF package) calculation of TAM-trianion.
(33) Strandberg, E.; Westlund, P. O. *J. Magn. Reson. A* **1996**, *122*, 179.

MA021105K